Journal of Hydrology 589 (2020) 125182

Contents lists available at ScienceDirect

Journal of Hydrology

journal homepage: www.elsevier.com/locate/jhydrol

Research papers

The role of extreme rain events in Peninsular Florida's seasonal hydroclimate variations

Shangyong Shi[a], Vasubandhu Misra[a,b,c,*]

[a] Department of Earth, Ocean and Atmospheric Science, Florida State University, Tallahassee, FL, USA
[b] Center for Ocean-Atmospheric Prediction Studies, Florida State University, Tallahassee, FL, USA
[c] Florida Climate Institute, Florida State University, Tallahassee, FL, USA

ARTICLE INFO

This manuscript was handled by Marco Borga, Editor-in-Chief, with the assistance of Eylon Shamir, Associate Editor

Keywords:
Precipitation extremes
Florida hydroclimate
Seasonal predictability
ENSO

ABSTRACT

The role of extreme rains over Peninsular Florida (PF) in modulating the seasonal rainfall characteristics is investigated in this study. The paper is motivated on its potential implication on the seasonal predictability of the hydroclimate of PF by relatively coarse global seasonal climate models. A majority of these climate models are unable to resolve the weather events like tropical cyclones that produce such extreme rain events. Therefore, a legitimate question to ask is if this limits the model's seasonal predictability of the hydroclimate of PF.

In this paper, extreme rain events over PF within a season are defined as days with daily rain amount at or above the 95th percentile over 39 years from 1979 to 2017 at the grid resolution of the observed rainfall dataset ($0.5^{\circ} \times 0.5^{\circ}$). The thresholds for extreme rain days range from 16 $mmday^{-1}$ to 36 $mmday^{-1}$ depending on the season and the location over PF, while the heaviest rainfall range from 58 $mmday^{-1}$ to 278 $mmday^{-1}$. These extreme rain events occur most often across PF in the boreal summer season followed by the fall season with the least in the boreal winter season. Our study reveals that removing the days of extreme rain events has the largest impact on the corresponding seasonal anomalies and daily rainfall distribution in the dry winter season and least in the wet summer season.

The impact of El Niño and the Southern Oscillation (ENSO) on the extreme rain events was evaluated by contrasting the differences in the shape and the scale parameters of the fitted Gamma distribution on daily rainfall in winter/spring seasons during warm and cold phases. Results revealed that the warm ENSO phases make the tails of the daily rainfall distribution over PF heavier and longer relative to the cold ENSO phases in the winter and spring seasons. In essence, our study reveals that the extreme rain events that are critical for the overall seasonal distribution of rainfall over PF in the first half of the year is modulated by large-scale phenomenon (e.g., ENSO). In the latter half of the year (summer and fall), the extreme rain events are not as critical to the seasonal rainfall anomaly or the overall seasonal distribution of rainfall over PF. Therefore, resolving the extreme rain events need not be as critical for the seasonal predictability of the hydroclimate of PF.

1. Introduction

Extreme rain events are well known for their potential to lead to collateral damage and human fatalities. There is considerable interest to understand these extreme rain events, especially in the US, where they are known to cause considerable damage (Schumacher and Johnson, 2005, 2006; Curtis, 2008). For example, Schumacher and Johnson (2006) examined rain gauge observations east of the Rockies and outside of Florida over five years (1999–2003) and found that a majority of the extreme rain events (defined as those that exceed 50-year recurrence interval) occurred in the month of July. They also established that nearly two-thirds of these events were associated with mesoscale convective systems and about a quarter of the events were related to synoptic weather systems. In a related study, Chan and Misra (2010) showed that anomalous wet summer seasons in the southeastern US is characterized by a greater number of heavy (> 10 mm/day) precipitation events than anomalous dry seasons. They further indicated that these heavy precipitation events contributed to more than half the seasonal total rainfall.

There is however an absence of studies that examine the role of extreme rain events in defining the hydroclimate over Peninsular Florida (PF), despite the fact that Florida is identified to be a region greatly affected by landfalling tropical cyclones (Knight and Davis, 2009; Klotzbach, 2011) and high lightning density (Hodanish et al.,

* Corresponding author at: Department of Earth, Ocean and Atmospheric Science, Florida State University, 1011 Academic Way, Tallahassee, FL 32306, USA.
E-mail address: vmisra@fsu.edu (V. Misra).

https://doi.org/10.1016/j.jhydrol.2020.125182
Received 26 March 2020; Received in revised form 1 June 2020; Accepted 9 June 2020
Available online 13 June 2020

1997; Lericos et al., 2002) that point to high thunderstorm activity. Some recent studies have examined the impact of climate change on rainfall extremes in Florida (Nadarajah, 2005; Wang et al., 2013) but they still do not fill the void of understanding the contribution of the extreme rain events on the seasonal hydroclimate of PF.

The strong seasonality of the rainfall in PF is well documented (Misra and DiNapoli, 2013; Misra et al., 2017; Misra and Bhardwaj, 2020). Ali et al. (2000) examined the spatial–temporal characteristics of monthly rainfall in central and south Florida and showed that the variance of the wet season (July) rainfall was far higher than that in the dry season (January). Similarly, in examining the spatial patterns of daily and monthly rainfall data in the tri-state area of Alabama, Georgia, and Florida, Baigorria et al. (2007) found two dominant spatial correlation patterns that suggested frontal type and convective thunderstorm events, which were characteristic of the dry and wet seasons, respectively. Keim (1996) analyzed heavy rainfall events (that produced over 75 mm of rainfall) across a much wider region of the southeastern United States (from Florida to Texas and North Carolina to Oklahoma) and concluded that frontal systems, particularly cold fronts, was the most dominant mechanism that induced heavy rainfall across the area. Moreover, tropical disturbances and air-mass thunderstorms were also found to be important, but largely confined to coastal locations.

A number of studies have examined the seasonal predictability over Florida, which generally indicate that the winter season has higher and useful prediction skills while in the summer and fall seasons the models display relatively poor fidelity (Stefanova et al., 2012; Tian et al., 2014; Kirtman et al., 2017). However, the current climate models used to simulate Florida's climate are comparatively coarse in spatial resolution (~1° × 1°; e.g. Kirtman et al., 2014; Voldoire et al., 2019) and are inadequate to resolve the weather systems that produce such extreme rain events (Iorio et al., 2004; Li et al., 2012). Therefore, it is legitimate to ask if their seasonal prediction skills over Florida are affected without resolving some of these extreme rain events.

This paper is motivated to understand the contribution of extreme rainfall events to seasonal rainfall over Peninsular Florida (PF). We seek to identify 1) the role of extreme rainfall in modulating rainfall distributions in the different seasons, and 2) the impact of El Niño and the Southern Oscillation (ENSO) on extreme rainfall. We examine the impact of ENSO specifically because it is one of the most widely studied and well known interannual variations (Cane and Zebiak, 1985; Philander, 1990; Guilyardi et al., 2009; Capatondi et al., 2014) that impacts PF significantly (Ropelewski and Halpert, 1986, 1987; Bove et al., 1998; Misra et al., 2012; Nag et al., 2014). Additionally, considerable progress has been made on understanding and improving ENSO predictability (Guilyardi et al., 2009; Capatondi et al., 2014; Kumar et al., 2017; Chen et al., 2020).

We hope to provide a better perspective on the potential for seasonal predictability of the hydroclimate over PF from the analysis of the results of this study. In the following section we describe the datasets used and the methodology followed by discussion of results in Section 3. Concluding remarks are provided in Section 4.

2. Data and methodology

We use the daily rainfall data from the Climate Prediction Center (CPC) (Xie et al., 2007; Chen et al., 2008). This rainfall data is available on a 0.5° × 0.5° grid at daily interval from 01 January 1979 to 22 March 2018 over all continental regions. This dataset uses gauge reports from over 30,000 stations including those from Cooperative Observer network Program (COOP), and other national and international collections. A quality control is applied on these data collections before they are merged through an optimal interpolation technique following Gandin (1965) to construct the global gridded rainfall analysis on $0.5^{\circ}(\text{lat}) \times 0.5^{\circ}(\text{lon})$ grid. In comparison to previous CPC products, the CPC unified daily gauge analysis presents spatial patterns and temporal changes of precipitation in better agreements with station data (Xie et al., 2007). Chen et al. (2008) showed that continental US, including Florida, has the highest density of rain gauges in the world. The mean station-to-station distance is around 30 km and the bias is less than |0.5%|. In a comprehensive review of gridded rainfall analysis, Sun et al. (2018) finds that the largest uncertainties of gridded analysis are found in complex mountain areas and in regions of sparse data coverage (e.g. northern Africa, polar latitudes, oceanic regions). In contrast, the flat terrain and relatively high density of rain gauges ensure a higher fidelity of the rainfall analysis over Florida.

For this study we use the data only over PF with a spatial range of 84.25°W to 79.75°W and 24.75°N and 31.25°N. We examined the impact on the statistical moments and the daily rainfall distribution from the extreme rain events to provide a complete picture on the sensitivity of the extreme rain events on seasonal rainfall. The methodology is explained in four subsections that dwell on climatology, defining extreme rain events, fitting a Gamma distribution to the daily rainfall in the season and the significance test.

The methodology follows a textbook type analyses to provide insight to the daily rainfall distribution within the four seasons of the year over PF. This is followed by a sensitivity analysis to specifically examine the role of extreme rain events on defining the seasonal hydroclimate and its variations over PF.

2.1. Climatology

To examine climatological characteristics of the statistical moments, the 39-year mean rainfall was calculated for each season and its standard deviation, skewness, and kurtosis were computed based on this mean rainfall. The skewness (s) and kurtosis (k) were computed as:

$$s = \frac{\frac{1}{N}\sum_{i=1}^{N}(r_i - \bar{r})^3}{\left(\sqrt{\frac{1}{N}\sum_{i=1}^{N}(r_i - \bar{r})^2}\right)^3} \quad (1)$$

and

$$k = \frac{\frac{1}{N}\sum_{i=1}^{N}(r_i - \bar{r})^4}{\left(\sqrt{\frac{1}{N}\sum_{i=1}^{N}(r_i - \bar{r})^2}\right)^4} \quad (2)$$

where r_i is the daily rainfall and $\bar{r}$ is the seasonal mean rainfall.

2.2. Definition of extreme rainfall

Extreme rainfall days were defined when the daily rain rate was at or exceeded the 95th percentile for each season from 1979 to 2017 (Suppiah and Hennessy, 1998; Haylock and Nicholls, 2000; Klein Tank and Konnen, 2003). But instead of computing this percentile over only wet days ($> 0.1\ \text{mmday}^{-1}$) of the season, we took into account all days including dry days to avoid bias stemming from any changes to the frequency of wet days (e.g., Schär et al., 2016). To compute the thresholds, the daily rain rates for more than 3500 days for each grid were ranked in descending order, with the days of equal rain rate belonging to the same rank. Then the rain rate at the 95th percentile was defined as the threshold for extreme rainfall. In order to understand the impact of these rain events on the seasonal characteristics and daily rainfall distribution, we created a "modified" dataset where the rain days at or exceeding the 95th percentile threshold were zeroed out. All moments including the mean, standard deviation, kurtosis, and skewness were calculated for both the original and the modified dataset. Furthermore, the corresponding differences of these moments between the original and the modified data was also evaluated. The bootstrapping method (described in subsection d) was used to test the differences at 95% significance level.

2.3. Fitting daily rainfall with Gamma distribution

We also analyzed the frequency distribution of precipitation by fitting empirical functions to the Probability Density Function (PDF) of the daily precipitation over PF. Precipitation amounts are left-bounded by zero and skewed to the right. There are a lot of distributions that meet these two requirements, and Gamma distribution stands out with its versatility of shapes. Though in some regions, Gamma distribution doesn't work well (Vlček and Huth, 2009), it has been widely applied to daily or monthly precipitation time series to study regional precipitation characteristics (Wilks, 2006; Becker et al., 2009; Husak et al., 2009).

The Gamma distribution PDF, for a given variable $\times$ ($\in r$) is given by:

$$f(x) = \frac{(x/\beta)^{\alpha-1}e^{-x/\beta}}{\beta\Gamma(\alpha)},\ x,\ \alpha,\ \beta > 0 \tag{1}$$

whereα is the shape and β is the scale parameters of the distribution. $\Gamma(\alpha)$ is the Gamma function defined by:

$$\Gamma(\alpha) = \int_0^\infty e^{-t}t^{\alpha-1}dt \tag{2}$$

The shape and scale parameters need to be estimated from the data series. The maximum likelihood estimators (MLE) developed by Thom (1958) is used. The estimators $\hat{\alpha}$ and $\hat{\beta}$ are calculated as follows:

$$A = ln(\bar{x}) - \frac{1}{n}\sum_{i=1}^{n} ln(x_n) \tag{3}$$

$$\hat{\alpha} = \frac{1}{4A}\left(1 + \sqrt{1 + \frac{4A}{3}}\right) \tag{4}$$

$$\hat{\beta} = \frac{x}{\hat{\alpha}},$$

where n is the number of values in x, and A is the sample statistic, which is the difference between the logs of the arithmetic and the geometric means (Wilks, 2006). Since the sample statistic A contains natural log, zero values should be discarded from original data series. We determine the threshold for a wet day, t, *as* 0.1 mm/day, given that the measurable rain amount at an observation station is typically 0.1 mm (Groisman et al., 1999). At each grid, the frequency of wet days, *pw*, for each season is therefore defined as number of wet days divided by the number of days in the season in the 39-year period. The frequency of wet days in PF is usually larger than 0.3 (not shown).

An example of fitting Gamma distribution to the wet days at one grid is provided in Fig. 1. A wet day threshold of $t_e = 1$ mmday^{-1} was applied to better present the histograms. In removing the dry days, a zero frequency value is implied for the [0, t_e] interval. If we fit a Gamma distribution over such a rainfall distribution, the fitted PDF would start with zero, which creates a right-skewed, inverted-U shape function with a local maximum at x = t_e (Fig. 1a). To avoid such bias, we fit the Gamma distribution to (x − t_e). The difference of fitting to an unshifted and a shifted data series is shown in Fig. 1. As a consequence of shifting the distribution, the shape of the fitted PDF changes to an exponential decay (Fig. 1b), and the shape parameter drops from larger than 1 (Fig. 1a) to below 1 (Fig. 1b). It should be noted that the shape parameter in the Gamma distribution is a measure of the skewness of the distribution with smaller values of α representing higher skewness in the distribution. It shows that, fitting the wet day data directly without dealing with the dry day frequency will lead to exaggeration of the shape parameter, which is the possible reason for a shape parameter of larger than 1 over most of US in Becker et al (2009).

Goodness-of-fit is tested using the Chi-square test following Wilks (2006). The null hypothesis H_0 is that the sample data at each grid is drawn from the estimated Gamma distribution. In this study, the sample data refers to the wet day data. The data is divided into unequal classes or bins, and each bin is ensured to have at least 5 values. The test statistic is computed as:

$$\chi^2 = \sum_{bins} \frac{(\#Observed - \#Expected)^2}{\#Expected} \tag{5}$$

$$= \sum_{bins} \frac{(\#Observed - n{\bullet}pw{\bullet}\Pr\{datainbin\})^2}{n{\bullet}pw{\bullet}\Pr\{datainbin\}} \tag{6}$$

where *(# Observed)* and *(# Expected)* correspond to the actual and computed counts of data values falling into each bin. The *# Expected* is equal to the cumulative probability (*pw*) in that bin multiplied by the sample size = *pw*•*n*, where, *n* is the number of wet days. A large χ^2 suggests that at least a few of the bins exhibit large discrepancies between the expected and observed counts, and that the fit is not good enough, leading to a rejection of the null hypothesis. The rejection level is determined by the degrees of freedom and the significance level. In this study, we use a rejection level of 0.05, meaning that we reject the null hypothesis at locations with *p*-values less than 0.05. The degrees of freedom of the time series at each grid point is estimated by the typical duration of synoptic scale systems, which is ~4 days (Holton and Hakim, 2013). Typically, in the summer season and in other seasons over PF when the duration of precipitation events is shorter (Bastola and Misra, 2013), the actual degrees of freedom will be larger than 4 days. Therefore, our choice of 4 days for the degrees of freedom serves as a more conservative estimate of χ^2.

2.4. Significance tests

The differences of the higher moments and the Gamma distribution

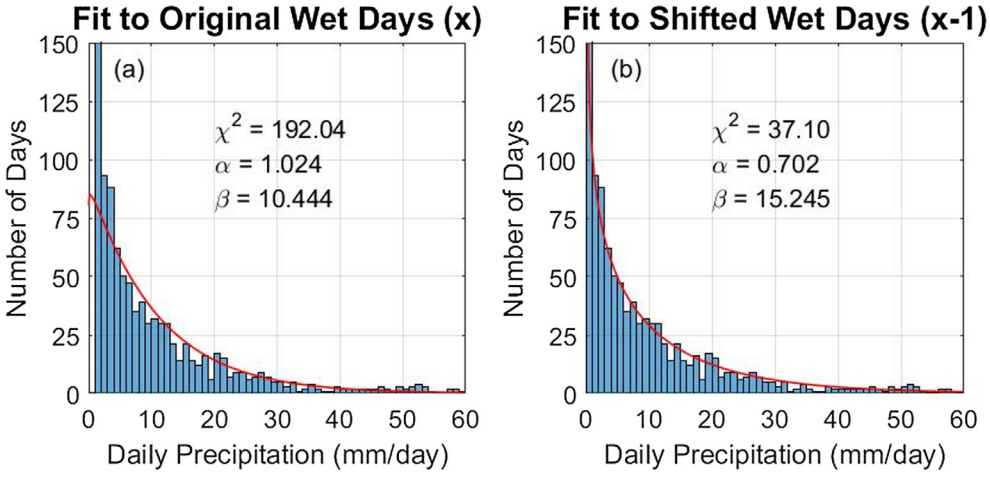

Fig. 1. An illustration of the two ways in fitting a Gamma distribution to daily precipitation at one specific grid point located over PF (83.75°W, 30.25°N). Fitting a Gamma distribution in which (a) a threshold to define wet day (as days with precipitation amount > 1 mm/day) is used to construct the histogram that artificially creates a bin with zero frequency in the precipitation interval between 0 and 1 mm/day and (b) the histograms are shifted (x-1) so that the first bin with zero frequency that appears in (a) is not included. The shape (α) and scale (β) parameters are estimated by MLE (Thom, 1958).

parameters before and after removing the extreme rain events were compared and tested by the bootstrapping method (following McClave and Dietrich (1994) and Efron and Tibshirani, 1993). For each grid point in each season, the number of extreme rain days were defined by the 95th percentile thresholds. After randomly deleting the same number of days in one season, we calculated the higher moments and the Gamma distribution parameters of the resampled seasonal rainfall data. The differences of these higher moments and the Gamma distribution parameters of the resampled rainfall data from the original sample were computed. This process was repeated for 200 times. Then the differences were ranked in descending order to determine the upper 2.5% and the lower 2.5% thresholds for the significance test. We claimed the statistical significance of the sensitivity of the extreme rain events on the higher moments or the distribution parameters at the 5% significance level when their rank fall either in the upper or in the lower 2.5% of the threshold.

We also examined the impact of El Niño and the Southern Oscillation (ENSO) phases on the Gamma distribution parameters of the daily rainfall in the boreal winter and spring seasons. The warm and cold ENSO phases were defined by a threshold of ± 0.5 °C for the Oceanic Niño Index (ONI) from Climate Prediction Center. 13 warm December-January-February's (DJF's) and 13 cold DJF's, 7 warm March-April-May's (MAM's) and 6 cold MAM's were identified. We fit the Gamma distribution to the daily rainfall distribution in each of these seasons separately. Bootstrapping method is used to test the differences of the shape and the scale parameters between the warm and cold phases of ENSO at the 5% significance level, similar to the process mentioned before.

3. Results

3.1. Seasonal climatology of rainfall over PF

The seasonal mean climatological rainfall in Fig. 2a-d clearly indicate that PF receives the most rainfall in the June-July-August (JJA) season followed by that in the September-October-November (SON) season. It is interesting to note that Gulf coast of PF receives the most rainfall in the JJA season (Fig. 2c) while in the SON season the Atlantic coast and the southern tip of PF receive the most rainfall (Fig. 2d). The December-January-February (DJF) season is the driest, especially, in South Florida (Fig. 2a) followed by the March-April-May (MAM) season. The seasonality of the rainfall north of 30°N over PF is relatively weak with comparable seasonal rainfall in DJF, MAM, and SON seasons, although, in JJA there is a visible annual peak. The corresponding standard deviation of the seasonal rainfall in Fig. 2e-h indicate that the JJA season displays the most variability across PF. The Atlantic coast and the southern tip of PF display relatively strong variability in the SON season (Fig. 2h) while in the DJF (Fig. 2e) and MAM (Fig. 2f) seasons the variability is stronger north of 28°N.

The skewness of the seasonal rainfall in Fig. 2i-l indicate that the DJF season is most positively skewed, which is understandable given that it is the driest season, which reduces the seasonal mean rainfall and deviations about this mean are amplified in the skewness. However, the MAM season, which was found to be also a dry season (Fig. 2b), shows far less skewness than the DJF season. In fact, the skewness of the daily rainfall in the rest of the seasons other than DJF is comparable. This potentially suggests that the tails of the daily rainfall distribution in these seasons are not relatively as heavy and or long as the DJF season. This may however have to be tempered with the fact that the heaviest rain rates occur in JJA season but is not reflected in the skewness because the seasonal mean rain is comparatively higher than in the DJF season. The kurtosis in Fig. 2m-p also indicate the DJF season with the largest values while it is comparable in the rest of the seasons. This supports the idea of relatively high frequency of dry days in the DJF season that result in a higher peak in the daily rainfall distribution of the season. Additionally, the higher kurtosis in the DJF season compared to other seasons also suggests a heavier and or a longer tail in the daily rainfall distribution of the DJF season.

3.2. Extreme rainfall over PF

As noted before the selection of extreme rainfall events is based on daily rainfall at or exceeding the 95th percentile threshold with the percentile computed by including all days of the season (including dry days). The climatological rain rate at the 95th percentile threshold for all four seasons is shown in Fig. 3a-d. Interestingly, Fig. 3a-d show that the threshold of rain rate at the 95th percentile is largest in the DJF and the MAM seasons, especially, north of 30°N with comparatively much lower thresholds in the JJA and the SON seasons. This result is partially a consequence of the JJA and the SON seasons having relatively more rainy days while DJF and MAM seasons have more dry day events. Since we assign the same rank for days with equal rain rate the threshold for the 95th percentile gets shifted to higher values when the rank order is shorter as in the dry seasons owing to a number of dry days. In south Florida, the threshold of the 95th percentile event is comparable in all four seasons. As a consequence, the meridional gradients of the threshold of the rain rates at the 95th percentile is strongest in DJF followed by that in the MAM season and weakest in JJA followed by that in the SON season (Fig. 3).

The percentage of days in the season when the daily rain rate exceeds the 95th percentile threshold is shown in Fig. 4a-d. The extreme rain events are most prevalent across PF in the JJA season with south Florida showing the highest frequency, followed by the SON season, with a relatively moderate decrease in the frequency over southwest PF and a larger decrease towards north of 28°N. The DJF season (Fig. 4a), followed by the MAM season (Fig. 4b), has the least frequency of the extreme rain events.

In order to understand the impact of these extreme rain events on the seasonal rainfall, we created a new dataset, wherein, we zeroed out the rainfall on days of the extreme rain events. We then examined the differences of these various statistics of this modified data series with the original data set to assess the impact of the extreme rain events on the seasonal rainfall over PF. The climatological seasonal mean rainfall differences (shown as original-modified) between the two data sets in Fig. 5a-d clearly shows that in the absence of the extreme rain events, the seasonal mean rainfall declines in a statistically significant manner across PF in all four seasons. Furthermore, the differences in Fig. 5e-h reveal that the variability of the seasonal rainfall across PF as defined by the standard deviation also declines with the absence of the extreme rainy days. Likewise, the differences in skewness (Fig. 5i-l) and kurtosis (Fig. 5m-p) also show a significant decrease when extreme rainy days are absent. The relatively large differences of these metrics in the dry seasons (DJF and MAM) indicate the relative importance of these extreme rain events on the mean state of the rainfall. In the MAM season when both skewness (Fig. 5j) and kurtosis (Fig. 5n) increase between Tampa and Orlando in the modified data series, it suggests that the mean state of the rainfall decreases considerably from the absence of these extreme rain events, which results in higher skewness and kurtosis in the modified dataset yielding a negative difference in Fig. 5j and n. In contrast, the relatively moderate changes to the skewness and kurtosis in the rest of the year (JJA and SON seasons) suggest the potential importance of the light to moderate rain events relative to the extreme rain events to the seasonal total.

These results have important implications on the seasonal predictability of the hydroclimate over PF. For example, it is well known that PF has the highest density of landfalling tropical cyclones in the continental US (Knight and Davis, 2009; Klotzbach, 2011). Therefore, one could claim that such extreme rain events could have an implication on the seasonal hydroclimate over PF during the Atlantic hurricane season. Yet when ENSO has a strong influence on the landfalling tropical cyclones over PF (e.g., Klotzbach, 2011; Misra et al., 2012; Kirtman et al., 2017) there is no discernible influence of ENSO on the seasonal

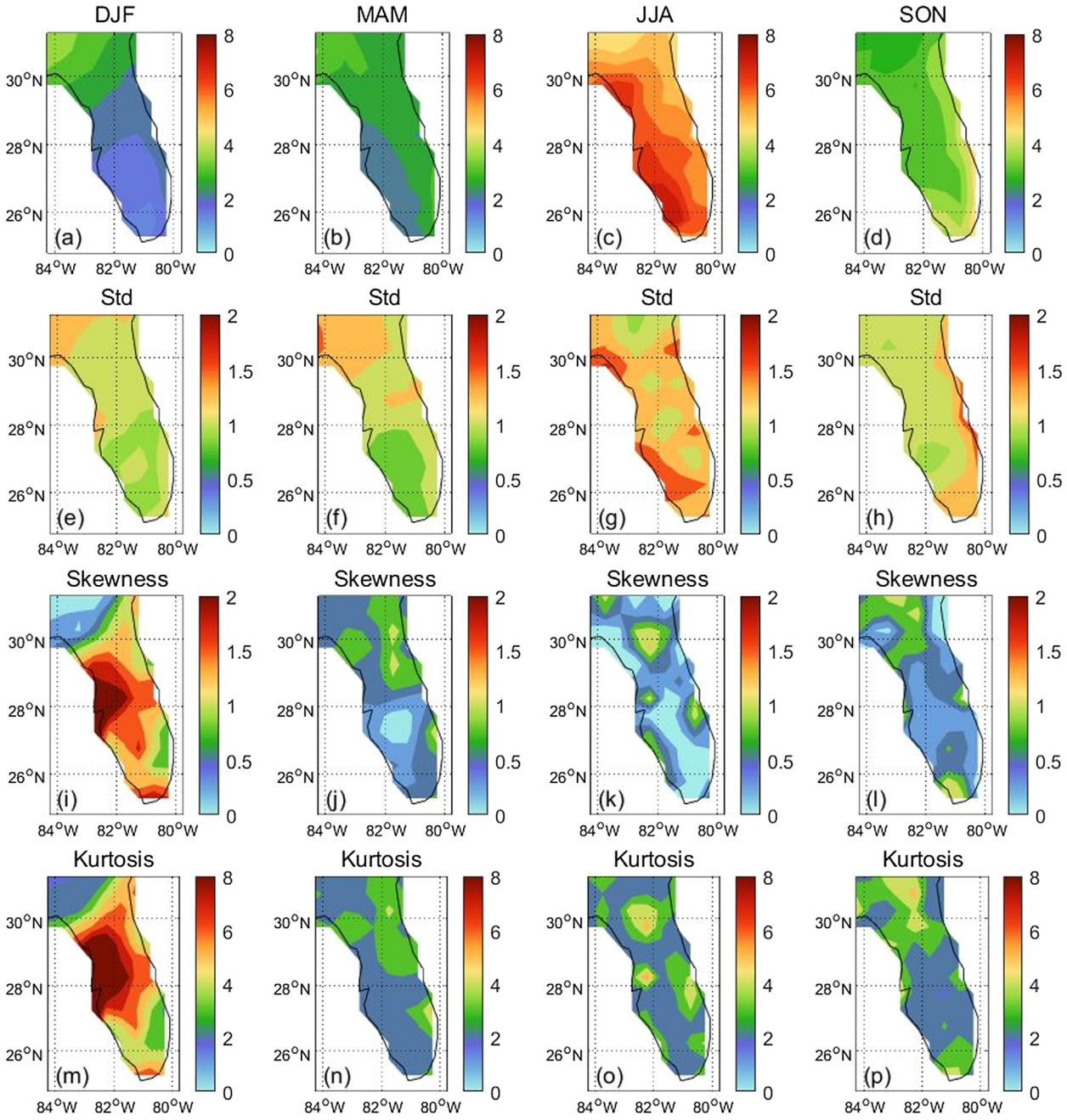

Fig. 2. The seasonal climatological (top row: a-d) mean rainfall (mm day^{-1}) and its corresponding (2nd row: e-h) standard deviation (mm day^{-1}), (3rd row: i-l) skewness and (4th row: m-p) kurtosis of the four seasons (DJF, MAM, JJA, and SON) based on daily gridded rainfall analysis from 1979 to 2017 (Xie et al., 2007; Chen et al., 2008).

precipitation anomalies of either the summer or the fall seasons over PF (Misra and DiNapoli, 2013; Kirtman et al., 2017). Our results corroborate these findings further in suggesting that the extreme rain events as isolated by those events ranked at or above the 95th percentile (which include these infrequent landfalling tropical cyclone events over PF) do not significantly contribute to the overall rainfall distribution of the corresponding season.

3.3. *Fitting the Gamma distribution to understand characteristics of extreme rain*

In order to put the findings of the previous sub-section on a more theoretical footing and to understand the contribution of the extreme rain events to the seasonal rainfall total in an alternative manner, we examined the characteristics of the fitted Gamma distribution to the daily rainfall distribution in each of the four seasons. As mentioned earlier, Gamma distribution is a two parameter frequency distribution described by the shape and the scale factors. The shape and scale factors inform the characteristics of the fitted Gamma distribution such that, shape dominated distributions suggest a weaker contribution of the extreme rains to the seasonal total vis-à-vis a scale dominated distribution that would imply a greater importance of the extreme rains to the seasonal total (Becker et al., 2009).

In Fig. 6a-d we show the shape parameter of the fitted gamma distribution for the daily rainfall of the four seasons. Similarly, Fig. 6e-h displays the corresponding scale parameter of the gamma distribution. Grids that don't pass the Chi-square test are masked out. There are many interesting observations from these figures that one could make

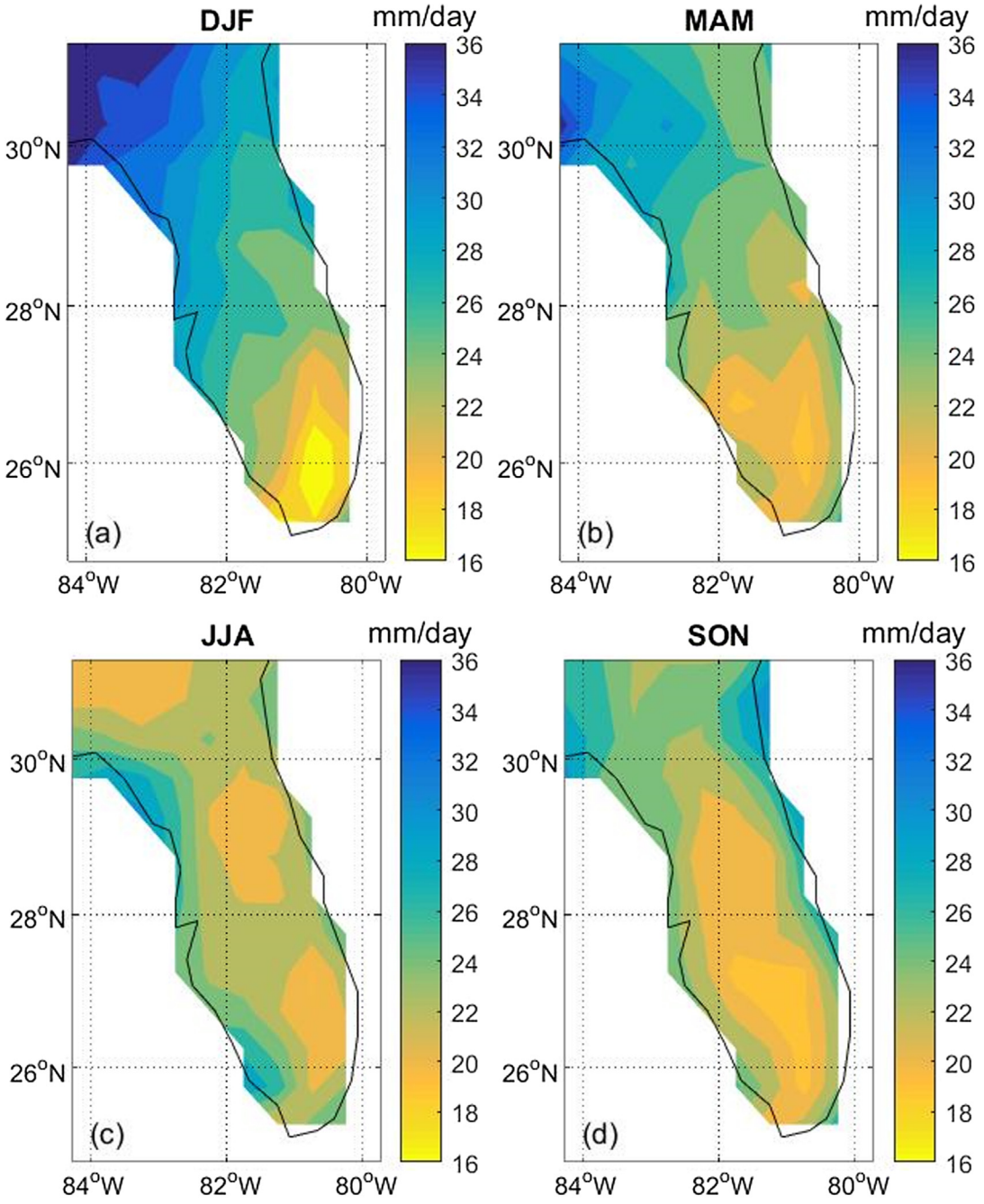

Fig. 3. The cutoff threshold for rain rates (mm day^{-1}) that are at or above the 95th percentile for a) DJF, b) MAM, c) JJA, and d) SON.

based on the spatial gradients of the shape and the scale parameters of the gamma distribution, including:

i) Gamma distribution is a good fit to daily rainfall distribution in all four seasons across most parts of PF.
ii) The daily precipitation in the DJF season shows a distribution with low shape parameter (pointing to comparatively larger skewness) that is evenly distributed across PF (Fig. 6a). At the same time, we observe in DJF that over northern Florida (north of 28°N) the distribution is scale dominated (suggesting heavier and or long tails) with their largest values appearing north of 30°N (Fig. 6e).
iii) Like in the DJF season, the shape parameter is small and uniformly distributed across PF in the MAM season (Fig. 6b). The distribution is scale dominated especially in northern parts of PF, which points to the significance of the extreme rain events to the seasonal total.
iv) In the JJA season the shape parameter assumes a larger value than in the previous two seasons (Fig. 6c) while the scale parameter diminishes (Fig. 6g), which connote that extreme rain events are comparatively less important and light to moderate rain rates contribute significantly to the seasonal total.
v) In the SON season the daily distribution of rainfall begin to revert to relatively smaller values of the shape parameter across PF (Fig. 6d) and larger values of the scale parameter (Fig. 6h) showing the growing importance of the extreme rain events on the seasonal total.

Now, we re-fit the gamma distribution on the modified data series where in the rain events at or exceeding the 95th percentile threshold is zeroed out to assess the importance of such events on the seasonal total (Fig. 7). The following inferences on the impact of the extreme rain

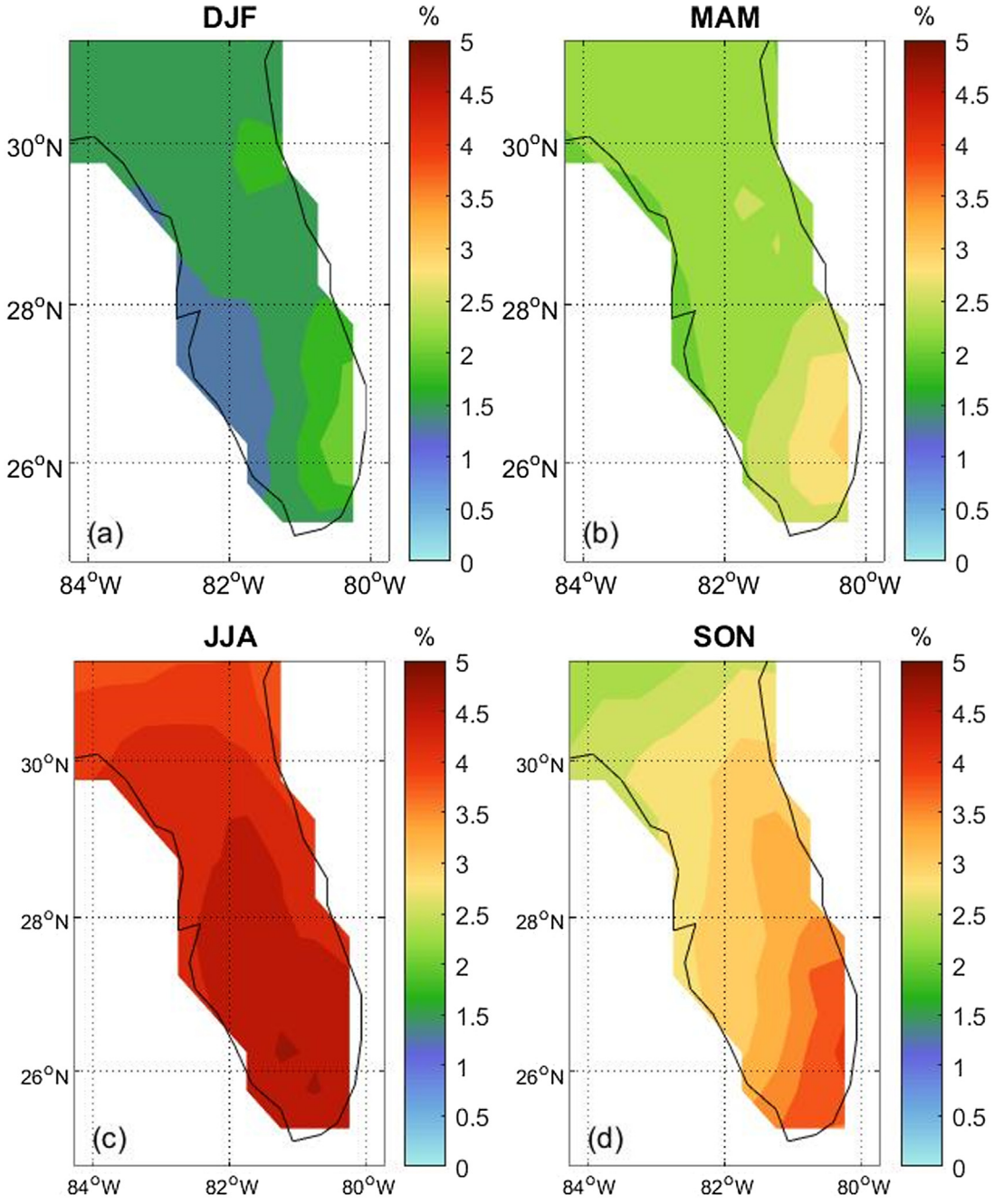

Fig. 4. The percentage of days in a) DJF, b) MAM, c) JJA, and d) SON when daily rain rates were at or above the 95th percentile.

events on the seasonal totals and the rainfall distribution in the season can be made from Fig. 7:

i) In each of the seasons the shape parameter increases, and the scale parameter declines in the modified data series relative to the original data. This suggests that the extreme rain events contribute significantly to the seasonal total in all four seasons across PF.
ii) Between the DJF and the MAM seasons, the impact of removing the extreme rain events is slightly higher in the MAM season relative to the DJF season, with larger changes observed to the shape and scale parameters in the MAM season.
iii) Between the JJA and the SON seasons, the shape parameter shows a larger impact in the former compared to the latter season with the JJA season assuming larger values of the shape parameter in the modified data series, which imply the growing influence of the light to moderate rain events on the seasonal total. However, in the SON season the scale parameter shows a larger reduction compared to the JJA season suggesting the diminishing influence of the extreme rain events on the seasonal total.

Bastola and Misra (2013) clearly showed that diurnal variations contribute significantly to seasonal rainfall over PF throughout the year. In JJA and SON seasons, diurnal variations explain nearly 50% of the total seasonal variance in parts of PF (Carbone and Tuttle, 2008; Bastola and Misra, 2013). These diurnal variations of precipitation are associated with sea-breeze type of thunderstorms (Blanchard and Lopez, 1985; Hodanish et al., 1997). Therefore, if the bulk of the seasonal rainfall comprises of such rain events, it is incumbent of the seasonal prediction models to simulate these diurnal variations with reasonable fidelity. However, the timing and magnitude of the diurnal variations is a challenging issue for climate models (Dai and Trenberth, 2004; Lewis and Karoly, 2013; Yin and Porporato, 2017; Wang et al.,

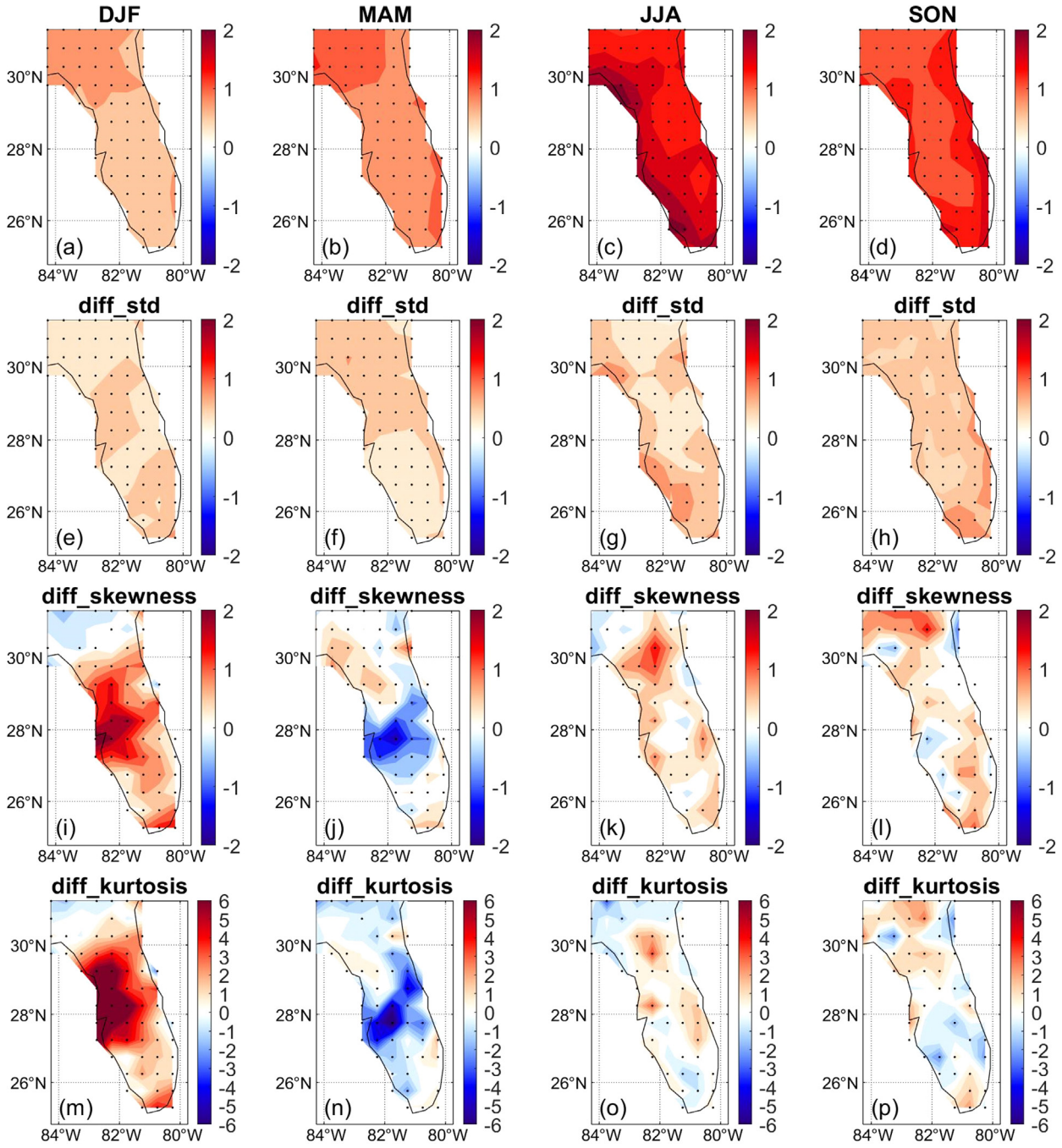

Fig. 5. The difference in the seasonal climatological (top row: a-d) mean (mm day^{-1}) and its corresponding (2nd row: e-h) standard deviation (mm day^{-1}), (3rd row: i-l) skewness and (4th row: m-p) kurtosis of the four seasons (DJF, MAM, JJA, and SON) of the modified rainfall data (wherein the days with rain rates at or above the 95th percentile is zeroed out) from the original data. The dots indicate that the (original-modified) differences are statistically significant at 95% confidence interval according to the bootstrap method.

2018). This issue is further accentuated over PF because the sea breeze events require much higher spatial resolution than the current climate models offer (Pielke, 1974; Anthes et al., 1982; Tijm et al., 1999). Our results show that extreme rain events make a relatively weak contribution towards the seasonal distribution of rainfall in the summer and fall seasons. The distribution of summer rainfall is not sensitive to extreme rain events, which are primarily produced by tropical cyclones. Thus, the results from our study suggest that the absence of resolving the tropical cyclones in our current climate models (e.g., Kirtman et al., 2014, Rebecca et al., 2017) may not be as detrimental for the seasonal simulation of summer rainfall over PF. However, these global climate models continued to display poor prediction skills in summer and fall seasonal rainfall over PF, suggesting that there are other responsible factors, like the poor simulation of the diurnal variations.

3.4. The role of El Niño and the Southern Oscillation (ENSO)

The shape and the scale parameters for the warm DJF and MAM seasons, and the corresponding differences between the warm and the cold phases for the two seasons are shown in Fig. 8. The Gamma distribution parameters for the warm DJF (Fig. 8a and b, respectively) and for the warm MAM (Fig. 8c and d, respectively) seasons are quite similar to the corresponding shape and scale parameters fitted over all seasons in Fig. 6. In comparing the corresponding differences of this

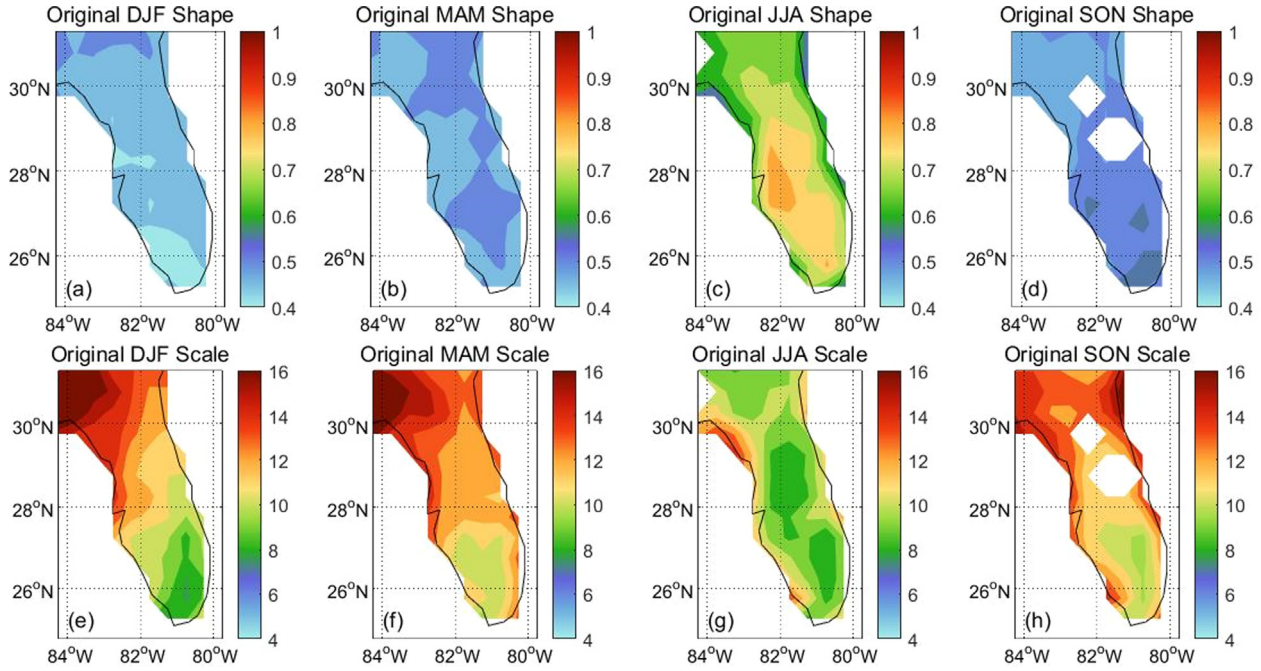

Fig. 6. The Gamma distribution (a, b, c, d) shape and (e, f, g, h) scale parameters fitted to the daily rainfall distribution in (a, e) DJF, (b, f) MAM, (c, g) JJA, and (d, h) SON seasons. The shaded values indicate that the Gamma distribution passes the goodness of fit according to the chi-squared test at 95% significance level except for the grey areas in (c), (g), (d) and (h).

distribution of shape and scale parameters with the cold ENSO phase seasons (Fig. 8e-h), we observe that in cold ENSO phases the scale parameter undergoes uniform reduction across PF in both seasons, while the changes to shape parameter is less conclusive. In other words, warm phase of ENSO tends to make the tails of the daily rainfall distribution heavier and or longer relative to the cold phase of ENSO. Given the importance of the extreme rain events in the daily rainfall distribution of the DJF and MAM seasons as revealed in the previous discussions, Fig. 8 further suggests that the ENSO forced signal in seasonal rainfall changes over PF can best be captured when these extreme rain events are resolved.

These results are significant in the context of the seasonal predictability of the hydroclimate of PF. As Kirtman et al. (2017) suggested, the remote ENSO forcing on the winter and spring seasonal climate over PF has a huge bearing on the fidelity of the seasonal prediction skills of the global models. Here, we find that ENSO also has a bearing on the

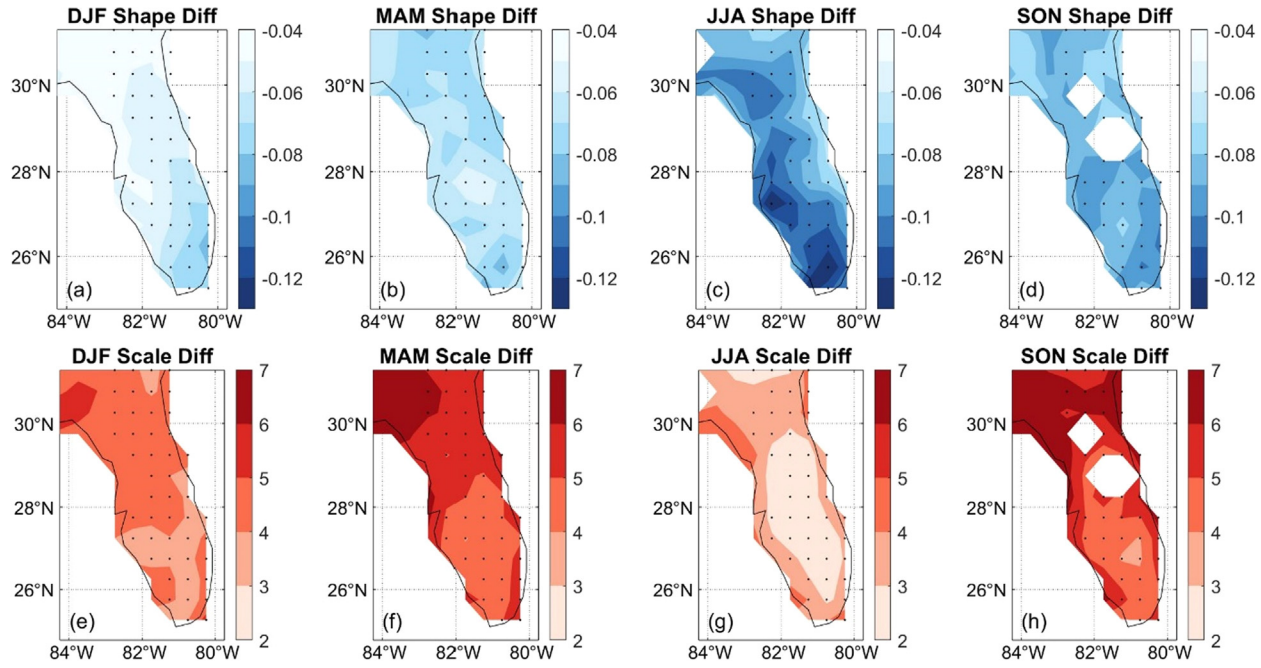

Fig. 7. The difference of Gamma distribution (a, b, c, d) shape and (e, f, g, h) scale parameters fitted to the modified daily rainfall distribution (original - modified), where in rain events at or exceeding the 95th percentile threshold is zeroed out in (a, e) DJF, (b, f) MAM, (c, g) JJA, and (d, h) SON seasons. The shaded values indicate that the Gamma distribution passes the goodness of fit according to the chi-squared test. The dots indicate that the differences are statistically significant at 95% confidence interval according to the bootstrap method.

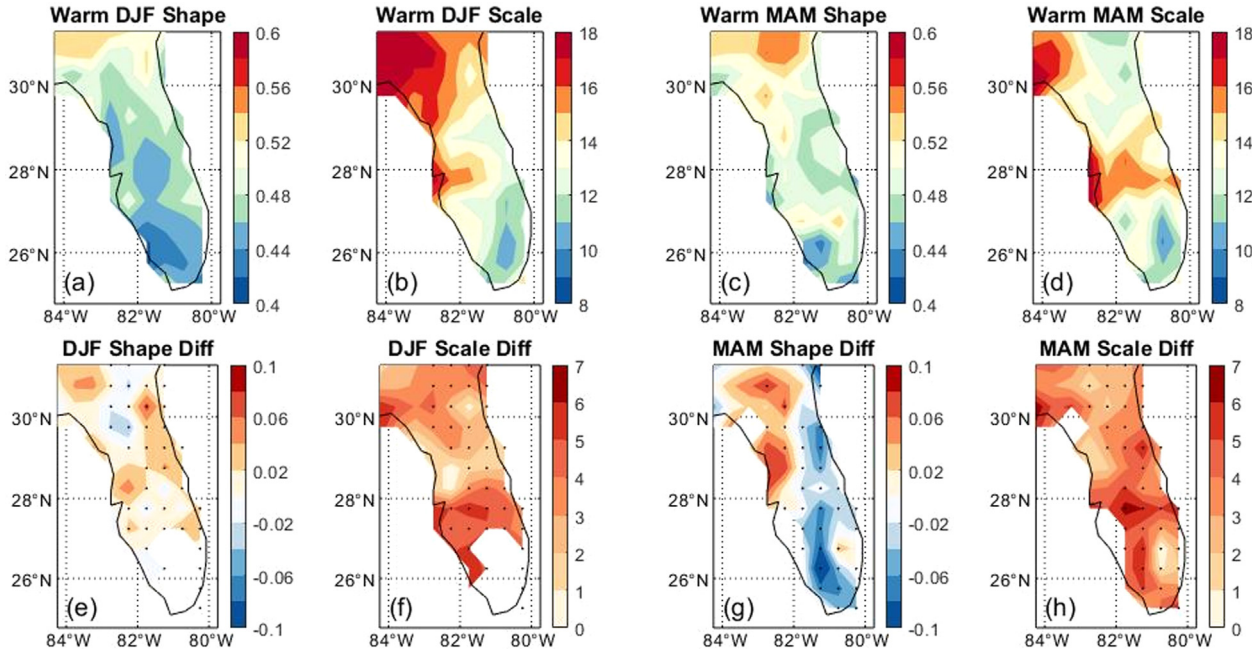

Fig. 8. The (a, c) shape and (b, d) scale parameters for the fitted Gamma distribution on the daily rainfall in the ENSO forced warm (a, b) DJF and (c, d) MAM seasons. The corresponding differences of (e, g) shape and (f, h) scale parameters of the Gamma distribution for ENSO forced warm-cold (c, d) DJF and (g, h) MAM seasons. The shaded values indicate that the Gamma distribution passes the goodness of fit according to the chi-squared test at 95% significance level. The differences in (e-h) are significant at 95% confidence interval according to the bootstrap method.

extreme rain events over PF in the DJF and MAM seasons and that such extreme rain events have a significant influence on the total rainfall distribution across the corresponding seasons. Therefore, our results suggest that these global seasonal climate models that display reasonable seasonal prediction skill over PF in these dry seasons are also resolving in all likelihood the variations in the frequency of these extreme rain events.

4. Conclusions

This paper has examined the daily rainfall distribution across PF in all four seasons. We examined the daily rainfall distribution over PF both by computing well known statistical metrics (e.g. skewness and kurtosis) and also by way of looking at the shape and scale parameters of the fitted Gamma distribution to the daily rainfall spread across the seasons.

Our results indicate that extreme rain events over PF are relatively more important to the seasonal total in the drier seasons of DJF and MAM, when the seasonal mean rainfall is small. This result is encouraging in that the extreme rain bearing systems in the boreal winter are usually from the synoptic frontal systems over this region (Ropelewski and Halpert, 1986, 1989; Kiladis and Diaz, 1989; Schmidt et al., 2001), that could be potentially resolved in relatively coarse climate models. As this study finds, these extreme rain events are strongly modulated by ENSO in the winter and spring seasons. Therefore, the global models, which display reasonable seasonal prediction skill in depicting ENSO teleconnections will likely pick this signal. However, in terms of long-term climate projections the uncertainty of projecting ENSO features like its frequency, duration, spatial structure in the equatorial Pacific Ocean in a future warm climate contribute to the uncertainty of extreme rain events and thereby the seasonal rainfall in the dry season over PF.

In the summer and fall seasons, PF has some of the largest fraction of landfalling tropical cyclones in the continental US. Yet we observe that the skewness and kurtosis of the daily rainfall distribution in the JJA and the SON seasons are relatively less modulated by the removal of these extreme rain events than in the drier DJF and MAM seasons. The seasonal distribution of rainfall in these seasons is largely made of light to moderate rain events that are related to diurnal variations (or sea-breeze type thunderstorm) events (Keim, 1996; Baigorria et al., 2007; Bastola and Misra, 2013). Therefore, the lack of resolving the tropical cyclones in coarse global climate models may not be detrimental to its seasonal prediction skill over Florida. However, unless the climate prediction models improve their simulation of light to moderate rain events there is little hope in improving the seasonal prediction skills or reducing the uncertainty in long-term climate projections of the summer and fall seasons hydroclimate over PF.

5. Data availability

The gridded rainfall dataset used in this paper can be publicly accessed from https://www.esrl.noaa.gov/psd/data/gridded/data.cpc.globalprecip.html.

The Oceanic Niño Index (ONI) is from Climate Prediction Center on https://origin.cpc.ncep.noaa.gov/products/analysis_monitoring/ensostuff/ONI_v5.php.

CRediT authorship contribution statement

Shangyong Shi: Methodology, Software, Visualization, Investigation, Validation, Writing - review & editing. **Vasubandhu Misra:** Conceptualization, Investigation, Writing - original draft.

Declaration of Competing Interest

The authors declare that they have no known competing financial interests or personal relationships that could have appeared to influence the work reported in this paper.

Acknowledgements

We acknowledge the support of NASA grant 80NSSC19K1199. The CPC Global Unified Precipitation data is provided by the NOAA/OAR/ESRL PSD, Boulder, Colorado, USA, from their Web site at https://

www.esrl.noaa.gov/psd/.

Appendix A. Supplementary data

Supplementary data to this article can be found online at https://doi.org/10.1016/j.jhydrol.2020.125182.

References

Ali, A., Abtew, W., Van Horn, S., Khanal, N., 2000. Temporal and spatial characterization of rainfall over Central and South Florida. J. Am. Water Resour. Assoc. 36 (4), 833–848.

Anthes, R.A., Keyser, D., Deardorff, J.W., 1982. Further consideration on modeling the sea breeze with a mixed-layer model. Mon. Wea. Rev. 110, 757–765.

Baigorria, G.A., Jones, J.W., Obrien, J.J.O., 2007. Understanding spatial rainfall variability in southeast USA at different timescales. Int. J. Climatol. 27, 749–760.

Bastola, S., Misra, V., 2013. Sensitivity of hydrological simulations of southeastern United States watersheds to temporal aggregation of rainfalls. J. Hydrometeor. 14, 1334–1344.

Becker, E.J., Berbery, E.H., Higgins, R.W., 2009. Understanding the characteristics of daily precipitation over the United States using the North American regional reanalysis. J. Clim. 22, 6268–6286.

Blanchard, D.O., Lopez, R.E., 1985. Spatial patterns of convection in south Florida. Mon. Wea. Rev. 113, 1282–1299.

Bove, M.C., Elsner, J.B., Landsea, C.W., Niu, X., O'Brien, J.J., 1998. Effects of El Niño on US landfalling hurricanes, revisited. Bull. Amer. Meteor. Soc. 79, 2477–2482.

Cane, M.A., Zebiak, S.E., 1985. A theory for El Niño and the Southern Oscillation. Science 228, 1085–1087.

Capatondi, A., Wittenberg, A.T., Newmann, M., Di Lorenzo, E., et al., 2014. Understanding ENSO diversity. Bull. Amer. Meteor. Soc. 96, 921–938. https://doi.org/10.1175/BAMS-D-13-00117.1.

Carbone, R.E., Tuttle, J.D., 2008. Rainfall occurrence in the U.S. warm season: the diurnal cycle. J. Clim. 21, 4132–4146.

Chan, S., Misra, V., 2010. A diagnosis of the 1979–2005 extreme rainfall events in the southeastern United States with Isentropic Moisture Tracing. Mon. Wea. Rev. 138, 1172–1185.

Chen, M., Shi, W., Xie, P., Silva, V.B.S., Kousky, V.E., Wayne Higgins, R., Janowiak, J.E., 2008. Assessing objective techniques for gauge-based analyses of global daily precipitation. J. Geophys. Res. 113, D04110. https://doi.org/10.1029/2007JD009132.

Chen, H., Tseng, Y., Hu, Z., et al., 2020. Enhancing the ENSO Predictability beyond the Spring Barrier. Sci. Rep. 10, 984. https://doi.org/10.1038/s41598-020-57853-7.

Curtis, S., 2008. The Atlantic multidecadal oscillation and extreme daily precipitation over the US and Mexico during the hurricane season. Clim. Dyn. 30, 343–351.

Dai, A., Trenberth, K.E., 2004. The diurnal cycle and its depiction in the Community Climate System Model. J. Clim. 17, 931–951.

Efron, B., Tibshirani, R.J., 1993. In: An Introduction to Bootstrap. Chapman and Hall, pp. 436.

Gandin, L.S., 1965. Objective analysis of meteorological fields. Israel Program Sci. Transl. 242, pp.

Groisman, P., Peck, E.L., Quayle, R.G., 1999. Intercomparison of recording and standard nonrecording U.S. gauges. J. Atmos. Oceanic Technol. 16, 602–609.

Guilyardi, E., Wittenberg, A., Fedorov, A., Collins, M., Wang, C., Capotondi, A., von Oldengorgh, G.J., Stockdale, T., 2009. Understanding El Niño in ocean–atmosphere general circulation models: progress and challenges. Bull. Amer. Meteorol. Soc. 90, 325–340.

Haylock, M., Nicholls, N., 2000. Trends in extreme rainfall indices for an updated high quality data set for Australia, 1910–1998. Int. J. Climatol. 20, 1533–1541.

Hodanish, S., Sharp, D., Collins, W., Paxton, C., Orville, R.E., 1997. A 10-yr monthly lightning climatology of Florida: 1986–95. Wea. Forecasting 12, 439–448.

Holton, J.R., Hakim, G.J., 2013. An Introduction to Dynamic Meteorology, fifth edition. Academic Press, pp. 540 pp..

Husak, G.J., Michaelsen, J., Funk, C., 2009. Use of the gamma distribution to represent monthly rainfall in Africa for drought monitoring applications. Int. J. Climatol. 27, 935–944. https://doi.org/10.1002/joc.

Iorio, J.P., Duffy, P.B., Govindasamay, B., Thompson, S.L., Khairoutdinov, M., Randall, D., 2004. Effects of model resolution and subgrid-scale physics on the simulation of precipitation in the continental United States. Clim. Dyn. 23, 243–258. https://doi.org/10.1007/s00382-004-0440-y.

Keim, B.D., 1996. Spatial, synoptic, and seasonal patterns of heavy rainfall in the Southeastern United States. Phy. Geogr. 17 (4), 313–328. https://doi.org/10.1080/02723646.1996.10642588.

Kiladis, G.N., Diaz, H.F., 1989. Global climatic anomalies associated with extremes in the Southern Oscillation. J. Clim. 2, 1069–1090.

Kirtman, B. P. et al., 2014: The North American Multimodel Ensemble. Bull. Amer. Meteor. Soc., 95, 585–601, DOI:10.1175/BAMS-D-12-00050.1.

Kirtman, B.P., Misra, V., Burgman, R.J., Infanti, J., Obeysekera, J., 2017. Florida climate variability and prediction. In: Chassignet, E.P., Jones, J.W., Misra, V., Obeysekera, J. (Eds.), Florida's Climate: Changes, Variations, & Impacts. Florida Climate Institute, Gainesville, FL, pp. 511–532. https://doi.org/10.17125/fci2017.ch17.

Klein Tank, A.M.G., Konnen, G.P., 2003. Trends in indices of daily temperature and precipitation extremes in Europe, 1946–99. J. Clim. 16, 3665–3680.

Klotzbach, P.J., 2011. El Niño-Southern Oscillation's impact on Atlantic basin hurricanes and U S. landfalls. J. Clim. 24, 1252–1263.

Knight, D.B., Davis, R.E., 2009. Contribution of tropical cyclones to extreme rainfall events in the southeastern United States. J. Geophys. Res. 114, D23102. https://doi.org/10.1029/2009JD012511.

Kumar, A., Hu, Z., Jha, B., Peng, P., 2017. Estimating ENSO predictability based on multi-model hindcasts. Clim. Dyn. 48, 39–51. https://doi.org/10.1007/s00382-016-3060-4.

Lericos, T.P., Fuelberg, H.E., Watson, A.I., Holle, R.L., 2002. Warm season lightning distributions over the Florida peninsula as related to synoptic patterns. Weather Forecast. 17, 83–98.

Lewis, S., Karoly, D.J., 2013. Evaluation of historical diurnal temperature range trends in CMIP5 models. J. Clim. 26. https://doi.org/10.1175/JCLI-D-13-00032.1.

Li, F., Rosa, D., Collins, W.D., Wehner, M.F., 2012. "Super Parameterization": a better way to simulate regional extreme precipitation? J. Adv. Mod. Earth Sys. 4 (2). https://doi.org/10.1029/2011MS000106.

McClave, J.T., Dietrich II, F.H., 1994. In: Statistics. MacMillan College Publishing Co., pp. 967.

Misra, V., Bhardwaj, A., 2020. The impact of varying seasonal lengths of the rainy seasons of India on its teleconnections with tropical sea surface temperatures. Atmos. Sci. Lett. e959. https://doi.org/10.1002/asl.959.

Misra, V., DiNapoli, S., Bastola, S., 2012. Dynamic downscaling of the 20th century reanalysis over the southeastern United States. Reg. Env. Change 13, S15–S23. https://doi.org/10.1007/s10113-012- 0372-8.

Misra, V., Bhardwaj, A., Mishra, A., 2017. Characterizing the rainy season of Peninsular Florida. Clim. Dyn. https://doi.org/10.1007/s00382-017-4005-2.

Misra, V., DiNapoli, S., 2013. Understanding the wet season variations over Florida. Clim. Dyn. 40 (5–6), 1361–1372.

Nadarajah, S., 2005. Extremes of daily rainfall in West Central Florida. Clim. Change 69, 325–342. https://doi.org/10.1007/s10584-005-1812-y.

Nag, B., Misra, V., Bastola, S., 2014. Validating ENSO teleconnections on Southeastern United States. Winter Hydrol. Earth Interact. https://doi.org/10.1175/EI-D-14-0007.1. In press.

Philander, S.G., 1990. El Niño, La Niña, and the Southern Oscillation. Academic Press, San Diego, CA.

Pielke, R.A., 1974. A three-dimensional numerical model of the sea breezes over south Florida. Mon. Wea. Rev. 102, 115–139. https://doi.org/10.1175/1520-0493(1974)102<0115:ATDNMO>2.0.CO;2.

Rebecca, A., Bolinger, A.D., Gronewold, K.K., Fry, L.M., 2017. Application of the NMME in the development of a new regional seasonal climate forecast tool. Bull. Amer. Meteor. Soc. 98, 555–564.

Ropelewski, C.F., Halpert, M.S., 1986. North American precipitation and temperature patterns associated with the El Niño Southern Oscillation (ENSO). Mon. Wea. Rev. 114, 2352–2362.

Ropelewski, C.F., Halpert, M.S., 1987. Global and regional scale precipitation patterns associated with the El Niño/Southern Oscillation. Mon. Wea. Rev. 115, 1606–1626.

Ropelewski, C.F., Halpert, M.S., 1989. Precipitation patterns associated with the high index phase of the Southern Oscillation. J. Clim. 2, 268–284.

Schär, C., et al., 2016. Percentile indices for assessing changes in heavy precipitation events. Clim. Change 137, 201–216. https://doi.org/10.1007/s10584-016-1669-2.

Schmidt, N., Lipp, E.K., Rose, J.B., Luther, M.E., 2001. ENSO influences on seasonal rainfall and river discharge in Florida. J. Climate 14, 615–628.

Schumacher, R.S., Johnson, R.H., 2005. Organization and environmental properties of extreme-rain-producing mesoscale convective systems. Mon. Wea. Rev. 133, 961–976.

Schumacher, R.S., Johnson, R.H., 2006. Characteristics of U. S. extreme rain events during 1999–2003. Wea. Forecasting 21, 69–85.

Stefanova, L., Misra, V., O'Brien, J.J., Chassignet, E.P., Hameed, S., 2012. Hindcast skill and predictability of APCC models for precipitation and surface temperature anomalies over the Southeast United States. Clim. Dyn. 38 (1–2), 161–173.

Sun, Q., Miao, C., Duan, Q., Ashouri, H., Sorooshian, S., Hsu, K.L., 2018. A review of global precipitation data sets: data sources, estimation, and intercomparisons. Rev. Geophys. 56 (1), 79–107. https://doi.org/10.1002/2017RG000574.

Suppiah, R., Hennessy, K.J., 1998. Trends in total rainfall, heavy-rain events and number of dry days in Australia, 1910–1990. Int. J. Climatol. 18, 1141–1164.

Thom, H.C.S., 1958. A note on the gamma distribution. Mon. Wea. Rev. 86, 117–122. https://doi.org/10.1175/1520-0493(1958)086<0117:anotgd>2.0.co;2.

Tian, D., Martinez, C.J., Graham, W.D., Hwang, S., 2014. Statistical downscaling of multi-model forecasts for seasonal precipitation and surface temperature over the Southeastern USA. J. Clim. 27, 8484–18411.

Tijm, A.B.C., Holtstag, A.A.M., van Delden, A.J., 1999. Observations and modeling of the sea breeze with the return current. Mon. Wea. Rev. 127, 625–640.

Vlček, O., Huth, R., 2009. Is daily precipitation Gamma-distributed? Adverse effects of an incorrect use of the Kolmogorov-Smirnov test. Atmos. Res. 93, 759–766. https://doi.org/10.1016/j.atmosres.2009.03.005.

Voldoire, A., et al., 2019. Evaluation of CMIP6 DECK experiments with CNRM-CM6-1. J. Adv. Mod. Sys. 11 (7), 2177–2213. https://doi.org/10.1029/2019MS001683.

Wang, H., Burleyson, C., Ma, P.-L., Fast, J.D., Rasch, P.J., 2018. Using the Atmospheric Radiation Measurement (ARM) datasets to evaluate climate models in simulating diurnal and seasonal variations of tropical clouds. J. Clim. 31, 3301–3325.

Wang, D., Hagen, S.C., Alizad, K., 2013. Climate change impact and uncertainty analysis of extreme rainfall events in the Apalachicola River basin, Florida. J. Hydrol. 480 (14), 125–135. https://doi.org/10.1016/j.jhydrol.2012.12.015.

Wilks, D.S., 2006. In: Statistical Methods in the Atmospheric Sciences. International Geophysics Series, 2nd edition. Academic Press, Burlington, MA, pp. 627.

Xie, P., Yatagai, A., Chen, M., Hayasaka, T., Fukushima, Y., Liu, C., Yang, S., 2007. A gauge based analysis of daily precipitation over East Asia. J. Hydrometeorol. 8, 607–626. https://doi.org/10.1175/JHM583.1.

Yin, J., Porporato, A., 2017. Diurnal cloud cycle biases in climate models. Nat. Commun. 8, 2269. https://doi.org/10.1038/s41467-017-02369-4.